IEEE Access
Multidisciplinary ⋮ Rapid Review ⋮ Open Access Journal

Received 15 March 2024, accepted 21 April 2024, date of publication 29 April 2024, date of current version 6 May 2024.

Digital Object Identifier 10.1109/ACCESS.2024.3395170

RESEARCH ARTICLE

A Variational Bayesian Approach for Channel Estimation in Pilot-Contaminated User-Centric C-RAN System

SOUMYASREE BERA, (Graduate Student Member, IEEE), VENU BALAJI VINNAKOTA, AND DEBARATI SEN, (Senior Member, IEEE)

G S Sanyal School of Telecommunications, Indian Institute of Technology Kharagpur, West Bengal 721302, India

Corresponding author: Soumyasree Bera (soumyasree.bera@gmail.com)

This work was supported by Indian Institute of Technology Kharagpur AI4ICPS I Hub Foundation under Grant TRP3RDEN01.

ABSTRACT In fifth-generation and beyond (5GB) wireless communication systems, Cloud Radio Access Network (C-RAN) is recognized as a vital technology. In this endeavor, User-Centric C-RAN (UC-RAN) promises a significant reduction in the channel training overhead because only the intra-cluster channel state information (CSI) is necessary for successful high data rate transmission. However, the network performance may be degraded by inter-cluster interference. Furthermore, such networks are susceptible to the pilot contamination effect, which leads to a major restriction on overall system performance. To tackle this issue, we introduce a channel estimation (CE) approach based on iterative variational Bayesian inference (IVBI)- called the least square IVBI (L-IVBI) scheme. This method consists of two stages: initialization and iteration, and is designed for the UC-RAN system. The initialization stage includes a coarse channel estimate, further refined in the iteration stage. We follow the alternative minimization method to estimate the desired channel in the iteration stage. Extensive simulation results for the UC-RAN system validate the proposed algorithms. We also provide the derivation of the Bayesian Cramer-Rao bound (BCRB) for the proposed estimator. The novel approach significantly outperforms the state-of-the-art in terms of normalized mean square error (NMSE), spectral efficiency (SE), and bit error rate (BER).

INDEX TERMS User-centric cloud radio access network, millimeter wave, channel estimation, iterative variational Bayesian inference, pilot contamination.

I. INTRODUCTION

The idea of a Cloud Radio Access Network (C-RAN) is to enhance the conventional Radio Access Network (RAN) architecture to improve Spectral Efficiency (SE), Energy Efficiency (EE), resource utilization, and Base Station (BS) utilization rate [1]. The C-RAN architecture consists of a Remote Radio Head (RRH) as a lighter version of the Base Station (BS), while the Base Band Unit (BBU) of various BSs is centralized in a location known as the BBU pool. The link that connects the RRHs to the BBU pool is called the fronthaul link, which can be either wired or wireless, depending on the traffic patterns of the specific geographic area and the resources available to the mobile operator [2]. The traditional cell-based network architectures are slowly moving towards clustering-based network architectures for 5G and beyond, where clustering involves Network Centering Cluster (NCC) [3] and User-Centric Cluster (UCC) methodologies. The User Equipment (UE) on the cell/cluster edge may still face outage issues with Cell and NCC clustering technologies. UCC technology offers seamless coverage and uniform Signal-to-Interference-Noise-Ratio (SINR) across all UEs, making it a popular choice. As the UCC is dynamic in nature, cooperation among BSs is necessary to keep it updated with respect to coverage availability at the UE [4]. The practical implementation of Coordinated Multipoint (CoMP) makes the C-RAN architecture the optimal choice for implementing UCC [5]. Hence, the combination of

The associate editor coordinating the review of this manuscript and approving it for publication was Olutayo O. Oyerinde.

C-RAN and UCC technologies is called User-Centric Cloud Radio Access Networks (UC-RAN).

The millimeter Wave (mmWave) communication is preferred in UC-RAN despite its problems, such as high propagation path loss, blockage issues, and hardware complexity [6]. This is because there is a large amount of available bandwidth in the mmWave spectrum, which provides high data rates [7]. Additionally, the short wavelength of mmWaves allows for implementing massive MIMO (mMIMO) technology, making it easier to place a greater number of antennas at the UE and RRH [8]. Therefore, utilizing mmWave-based UC-RAN can be highly beneficial, especially in indoor communications and ultra-dense networks. However, the technology also poses its own set of issues, such as the challenge of acquiring Channel State Information (CSI) [9]. The RRH's limited capacity to store and process CSI and the highly dynamic nature of the channel coefficients make CSI acquisition in UC-RAN difficult. Furthermore, interference from other UEs in the network, the large number of channels, and the dense deployment of RRHs add to the complexity of CSI estimation. As a result, real-time and accurate processing of channel estimation is crucial for the successful operation of UC-RAN [10].

The distinctive characteristics of UC-RAN, such as distributed signal processing and interference management, may render traditional CSI acquisition methods unsuitable. The most prevalent approach for acquiring CSI involves transmitting Uplink (UL) pilot signals, where a predetermined pilot signal is sent from the UE, and all RRHs can simultaneously estimate the channel response from the pilots [11]. When there is a need to estimate the channel response from multiple transmitting antennas, orthogonal pilot signals are generally required to differentiate the signals from the transmitting antennas [12]. Although pilot-based methods are popular, they are susceptible to pilot contamination, which arises when the pilots from various UEs in the UL interfere, leading to inaccurate CSI estimates. Even though UC-RAN systems have a distributed structure with relatively few antennas per RRH, making pilot contamination less of a concern compared to conventional mMIMO systems, it still cannot be ignored. To address this problem, several techniques have been proposed, including Pilot Assignment (PA), pilot power control, pilot decontamination, and pilot reuse, which take into account the careful design of pilot sequences.

A. BACKGROUND AND RELATED WORKS

In situations where more UEs are requesting access or being served across a particular carrier than the length of the pilot sequence, having an efficient PA policy becomes crucial. To achieve this, UC-RAN can implement PA policies that ensure co-pilot UEs are as far apart as possible while identifying which UEs require a dedicated pilot to minimize pilot contamination. A regular pilot reuse structure can be created through a clustering-based pilot assignment proposed in [13] to maximize the minimum distance between co-pilot UEs. This approach significantly reduces the pilot overhead required to keep pilot contamination at acceptable levels. However, optimizing the PA policy in UE-scheduling optimization problems [14], [15] becomes challenging when the number of UEs is significantly greater than available resources. Therefore, PA policies should rely on offline metrics such as UE locations, considering the overhead and computation complexity, to avoid wasting time constructing them.

In [16], the authors studied how to assign pilot sequences to control pilot contamination in a coexistence scenario of UC-RAN and D2D communication. They proposed two methods for pilot sequence assignment: the greedy algorithm [17] and the graph coloring-based algorithm [18], [19]. The greedy algorithm assigns the same pilot sequence to UEs with the minimum data rate to minimize the sum of the Large Scale Fading (LSF) coefficients, but it does not guarantee optimal performance as trying all combinations is impractical. In contrast, the graph coloring-based method selects co-pilot UEs individually to minimize potential interference and constructs an interference graph based on the LSF coefficients to achieve optimal pilot assignment among UEs. The results show a significant improvement in per-UE throughput compared to random pilot allocation schemes.

A graph-coloring theoretic approach is utilized to solve the PA problem in a user-centric clustered network in [20]. Another approach is presented in [21], which suggests a scheme based on the worst-performing UE and implements different stopping criteria for the pilot reassignment process. In [22], a framework is proposed to reduce pilot contamination by optimizing pilot transmission power through a min-max optimization problem. This problem aims to minimize the largest Normalized Mean Square Error (NMSE) of UEs and is solved using a sequential convex approximation method.

To mitigate the issue of pilot contamination, [23] put forward a technique based on Time of Arrival (TOA) that estimates the TOA of the multipath channel and then eliminates interfering signals from distant RRHs. This TOA-based channel estimation relies only on the current received signal and does not require channel statistics. Power control for the pilots can be implemented to enhance the accuracy of CSI estimation for reused pilots. Evaluation metrics for this technique could include the Bit Error Rate (BER) or Mean Square Error (MSE) of the channel [24]. Meanwhile, [25] introduced a Downlink (DL) training method for UC-RAN systems that improved achievable throughput significantly by utilizing max-min fairness-based power control. However, this study exclusively focuses on the use of mutually orthogonal DL pilots. Constructing a PA policy that reduces the pilot sequence length but takes considerable time to construct adds communication overhead, similar to using a longer pilot training period.

A Flexible Denoising Convolutional Neural Network (FFDNet) to address the high computational complexity associated with CSI estimation in mmWave unified UC-RAN is proposed in [26]. FFDNet is selected for its capacity to minimize training and testing latency while handling various noise levels using a single neural network [27]. To improve the quality of channel estimation by treating the channel matrix as an image, Convolutional Blind Denoising Network (CBDNet) is developed to enhance the denoising performance for noisy images encountered in real-world scenarios. In [28], the authors propose using CBDNet-based channel estimation for mmWave M-MIMO systems. A pilot utility-based method for assigning orthogonal pilots in UC-RAN using deep learning is presented in [29]. Reference [30] proposes ELM-based CE for enhancing RIS-assisted OFDM systems affected by insufficient CP and imperfect hardware, utilizing LS estimation and ELM networks with hidden-layer standardization. A joint model and data-driven receiver scheme for Data-dependent superimposed training (DDST), addressing symbol misidentification due to hardware imperfections is proposed in [31]. It combines linear receivers and nonlinear solutions, utilizing LS estimation, ZF equalization, and shallow neural networks (CE-Net and SD-Net) for improved channel estimation and data detection. In [32] authors explore the use of a Data-nulling superimposed pilot scheme to investigate the transfer learning (TL)-based Channel Estimation (CE) in Orthogonal Frequency Division Multiplexing (OFDM) systems, introducing a novel network called ReCNN. The proposed scheme combines Convolutional Neural Networks (CNN) to enhance the accuracy of Deep Learning (DL)-based CE by integrating linear and nonlinear solutions.

In UC-RAN, the limited capacity of RRH makes it challenging to train Deep Neural Network (DNN)s due to the need for a large amount of data. Therefore, there is a need for more efficient and scalable solutions for CSI acquisition. While Compressed Sensing (CS)-based channel estimation can reduce the overhead and latency associated with pilot-based channel estimation, it can be computationally intensive at the BBU and a bottleneck in frequently updating UC-RAN. To ensure the success of UC-RAN, the Bayesian Inference approach is crucial in accurately estimating the CSI using prior knowledge about the channel. In [33], a Bayesian approach that uses the covariance of channel vectors is employed to estimate CSI. The covariance matrix of channel vectors provides information about the mean and spread of multipath Angles of Arrival (AoAs) at the RRH. This approach is then used to develop a coordination protocol for assigning pilot sequences to UEs.

Researchers have proposed various classical algorithms for mmWave CE. One such algorithm is spatial grid-based OMP [34], sensitive to dictionary and stopping criteria. Another method, sparse Bayesian learning (SBL) [35], automatically determines non-zero elements, promising for joint estimation. However, deriving posterior PDF remains challenging. Variational inference [36], [37] approximates parameter posterior for mmWave MIMO channel estimation. The authors of [36] addressed the issue of detecting user activity and estimating channels within the fronthaul link of C-RANs. They presented Variational Bayesian Inference (VBI) that uses the sparsity of both user activity and signals spatial distribution. By employing a two-layer prior student's-t distribution graphical model, the proposed VBI algorithm mitigates bias. The VBI algorithm is widely used for estimating sparse vectors [38], and since the mmWave channel is inherently sparse, it may be employed for channel matrix estimation. However, VBI-based CSI estimation has not been implemented in a pilot-contaminated mmWave-based UC-RAN system. Inspired by the earlier discourse, we put forward a least square iterative variational Bayesian Inference (L-IVBI) channel estimation approach aimed at resolving the challenge of channel estimation in pilot-contaminated mmWave UC-RAN systems. This method capitalizes on the sparse nature of mmWave channels.

B. CONTRIBUTIONS

- The mathematical framework for user-centric pilot contaminated UC-RAN system over mmWave channel is designed.
- We introduce a Bayesian channel estimation algorithm called L-IVBI, designed specifically for the pilot-contaminated UC-RAN system. This algorithm approaches channel estimation as a sparse Bayesian problem, aiming to estimate both the desired and the integrated interfering channels from the superimposed signal using an alternate minimization technique. By computing posterior distributions for all hidden variables, our approach significantly enhances the accuracy of channel estimation compared to state-of-the-art methods.
- It eliminates the substantial overhead of estimating interfering clusters' large-scale fading coefficients. From the received symbols, an estimate of the sum of the large-scale fading coefficients of the interfering UEs is calculated.
- Additionally, we delve into the procedure of designing hybrid precoders and combiners based on the Orthogonal Matching Pursuit (OMP) algorithm for data transmission using the estimated channels.
- We derive a Bayesian Cramér-Rao Bound (BCRB) on the NMSE of the proposed estimator for the UC-RAN system. We observe through simulations that even at lower SNRs, our technique approaches the BCRB.

The remainder of this paper is organized as follows. Section II represents the system model of the user-centric C-RAN. In section III, the proposed L-IVBI channel estimation method is presented. Section IV presents the data transmission process utilizing designed hybrid precoding and combining followed by SE calculation. Section V provides the simulation results analysis, followed by the conclusion of the paper in section VI.

Notations: Matrix, vector, and scalar are denoted by $\mathbf{A}$, $\mathbf{a}$ and a respectively. The diagonal elements of the matrix $\mathbf{A}$ are represented by $diag[\mathbf{A}]$. Vectorization of matrix $\mathbf{A}$ is given as vec($\mathbf{A}$) and the inverse vectorization is denoted as vec$^{-1}(\mathbf{a})$. The symbols $\|\cdot\|_F$, $(\cdot)^H$, $(\cdot)^T$, $\otimes$, $\langle\cdot\rangle$, and $\|\cdot\|_2$ denote the Frobenius norm, Hermitian, transpose, Kronecker product, the expected value of the argument, and l_2 norm respectively.

II. SYSTEM MODEL

We consider a UC-RAN system with K' user equipment (UE) and a group of I' spatially distributed RRHs, where each RRH and UE are equipped with N_R and N_T antennas, respectively. As illustrated in Fig. 1, the user-centric cluster technique is considered, where nearby $I \in I'$ RRHs serve each UE exclusively since the signals received by the UE from distant RRHs are weak in nature due to the severe path loss. Furthermore, each RRH is assumed to be connected to the BBU pool via wireless fronthaul links. We consider an uplink (UL) transmission session comprising $K \in K'$ UEs with the same pilot sequences. The CSI of the target cluster becomes contaminated by the channels of $K-1$ interfering clusters due to pilot contamination caused by the unity pilot reuse factor. For simple system formulation, we assume cluster-1 as the desired/target cluster and the remaining $K-1$ clusters as interfering clusters. Furthermore, we assume that there is no cooperation among clusters.

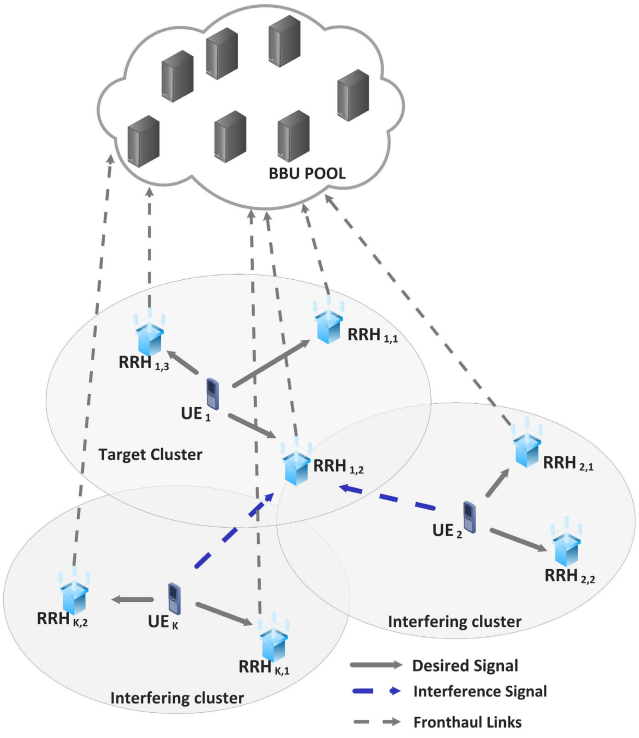

FIGURE 1. User-centric C-RAN Schematic diagram.

The transmission packet structure shown in Fig. 2 comprises a training frame consisting of pilots for CE followed by a data frame. First, each RRH uses the training frame

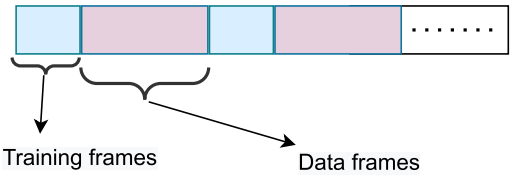

FIGURE 2. Packet transmission format.

transmitted by the UEs to perform channel estimation using the proposed methodologies. It is assumed that during this phase, there is no beamformation. Following CE, the corresponding CSI is transmitted through control channels to the UEs. Next, the data transmission phase starts that involves the hybrid analog and digital (HAD) structure for beamformation as shown in Fig. 3. Hence, the precoders and combiners are designed at each node utilizing the estimated CSI. N_S is the number of data streams, N_T and M_T are the number of transmitting antennas and RF chains, M_R and N_R are the number of receiving RF chain and antennas respectively. For the data transmission, utilizing the estimated CSI, each node obtains its respective hybrid analog or radio frequency (RF) and digital or baseband (BB) precoders and combiners.

Let $\mathbf{s}_k(n)$ denote the transmitted signal vector from k-th UE at time slot n. We assume the channel exhibits quasi-static behavior, meaning it remains constant throughout each transmission frame and varies independently across different frames. Each UE employs both BB and RF precoders to encode its data. Consequently, after applying the BB precoder matrix $\mathbf{W}_{BBT_k} \in \mathbb{C}^{M_T \times N_S}$ and the RF precoder matrix $\mathbf{W}_{RFT_k} \in \mathbb{C}^{N_T \times M_T}$, the transmitted signal at the n-th time instance from the user node $\mathbb{UE}_k$ can be expressed as follows:

$$\mathbf{x}_k(n) = \sqrt{p_k}\mathbf{W}_{RFT_k}\mathbf{W}_{BBT_k}\mathbf{s}_k(n), \tag{1}$$

where, p_k and $\mathbf{s}_k(n) \in \mathbb{C}^{N_S \times 1}$ denotes the transmitted power and data of node $\mathbb{UE}_k$ respectively. The signal vector, denoted by $\mathbf{y}_{1,i}(n) \in \mathbb{C}^{N_R \times 1}$, received at the i-th RRH of the targeted cluster i.e. $\mathbb{UE}_1$ is given as,

$$\begin{aligned}\mathbf{y}_{1,i}(n) &= \sum_{k=1}^{K}\mathbf{H}_{k,i}\mathbf{x}_k(n) + \mathbf{w}_{1,i}(n) \\ &= \underbrace{\mathbf{H}_{1,i}\mathbf{x}_1(n)}_{target\ cluster} + \underbrace{\sum_{k=2}^{K}\mathbf{H}_{k,i}\mathbf{x}_k(n)}_{interfering\ clusters} + \mathbf{w}_{1,i}(n),\end{aligned} \tag{2}$$

where, $\mathbf{w}_{1,i}(n) \in \mathbb{C}^{N_R \times 1} \sim \mathcal{CN}\left(0, \sigma_{w_i}^2\right)$ is the complex additive white Gaussian noise (AWGN) vector at i-th RRH of cluster-1. $\mathbf{H}_{k,i} \in \mathbb{C}^{N_R \times N_T}$ is the mmWave channel matrix between the k-th UE and i-th RRH defined as,

$$\mathbf{H}_{i,k} = \sqrt{\frac{N_T N_R}{N_{cl}}}\beta_{k,i}^{1/2}\sum_{l=1}^{N_{cl}}\alpha_l \mathbf{a}_R\left(\phi_l\right)\mathbf{a}_T^H\left(\theta_l\right), \tag{3}$$

where N_{cl} signifies the number of scatterers within the corresponding channel. $\beta_{k,i}$ represents the large-scale fading

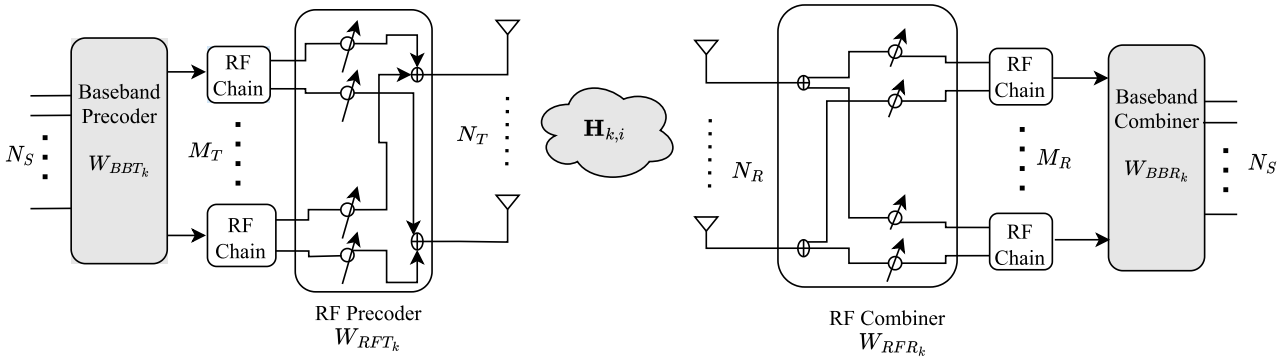

FIGURE 3. Illustration of hybrid precoding structure between UE and RRH.

coefficient between the k-th User Equipment (UE) and the i-th Remote Radio Head (RRH). The complex channel gain of the l-th path is denoted by $\alpha_l \in \mathbb{C}$. Additionally, $\theta_l \in [0, 2\pi)$ and $\phi_l \in [0, 2\pi)$ correspond to the Angle of Departure (AoD) and Angle of Arrival (AoA) of the l-th path, respectively. The steering vectors for the uniform linear receive and transmit array antennas, $\mathbf{a}_R(\phi_l) \in \mathbb{C}^{N_R \times 1}$ and $\mathbf{a}_T(\theta_l) \in \mathbb{C}^{N_T \times 1}$, are defined as follows:

$$\begin{aligned}&\mathbf{a}_R(\phi_l)\\&= \frac{1}{\sqrt{N_R}}\left[1, e^{-j\frac{2\pi}{\lambda}d_R cos\,\phi_l}, \ldots, e^{-j\frac{2\pi}{\lambda}(N_R-1)d_R cos\,\phi_l}\right]^T,\\&\mathbf{a}_T(\theta_l)\\&= \frac{1}{\sqrt{N_T}}\left[1, e^{-j\frac{2\pi}{\lambda}d_T cos\,\theta_l}, \ldots, e^{-j\frac{2\pi}{\lambda}(N_T-1)d_T cos\,\theta_l}\right]^T,\end{aligned} \tag{4}$$

where λ, d_T, and d_R represent the operating wavelength, transmit and receive antenna spacing, respectively. $\mathbf{H}_{k,i}$ in (3) can be written in a more compact way as [34],

$$\mathbf{H}_{k,i} = \widetilde{\mathbf{A}}_R \mathbf{G}_{v_{k,i}} \widetilde{\mathbf{A}}_T^H, \tag{5}$$

where, $\widetilde{\mathbf{A}}_R \in \mathbb{C}^{N_R \times N_{cl}}$ and $\widetilde{\mathbf{A}}_T \in \mathbb{C}^{N_T \times N_{cl}}$ consist of the array steering vectors $\mathbf{a}_R(\phi_l)$ and $\mathbf{a}_T(\theta_l)$ respectively and $\mathbf{G}_{v_{k,i}} = diag(\{C\}_l) \in \mathbb{C}^{N_{cl} \times N_{cl}}$ denotes a diagonal matrix with non-zero complex entries, where $\{C\}_l = \beta_{k,i}^{1/2}\alpha_l$. The sparse mmWave channel model is developed by partitioning of the AoD and AoA spaces spanning the interval $[0, \pi)$ with grids Θ_R and Φ_R, consisting $G_R, G_T \geq \max(N_R, N_T)$ angles, respectively. The quantized angles $\{\theta_g \in \Theta_R, \forall 1 \leq g \leq G_T\}$ and $\{\phi_g \in \Phi_R, \forall 1 \leq g \leq G_R\}$ are selected from the following conditions [34],

$$\begin{aligned}cos(\phi_g) &= \frac{2}{G_R}(g-1) - 1, \quad \forall 1 \leq g \leq G_R\\ cos(\theta_g) &= \frac{2}{G_T}(g-1) - 1, \quad \forall 1 \leq g \leq G_T.\end{aligned} \tag{6}$$

Therefore, the beamspace representation of the mmWave channel $\mathbf{H}_{k,i}$ is given as,

$$\mathbf{H}_{k,i} = \mathbf{A}_R \mathbf{G}_{k,i} \mathbf{A}_T^H, \tag{7}$$

where, $\mathbf{A}_R \in \mathbb{C}^{N_R \times G_R}$ and $\mathbf{A}_T \in \mathbb{C}^{N_T \times G_T}$ contain the receiver and transmitter array response vectors calculated on G_T for the AoD and G_R for the AoA. $\mathbf{G}_{k,i} \in \mathbb{C}^{G_R \times G_T}$ is a sparse matrix equivalent to the channel matrix $\mathbf{H}_{k,i}$.

At the i-th RRH of cluster-1, the received signal $\mathbf{y}_{1,i}(n)$ from (2) is then processed by RF and BB combiners $\mathbf{W}_{RFR_k}$ and $\mathbf{W}_{BBR_k}$ given as,

$$\breve{\mathbf{y}}_{1,i}(n) = \mathbf{W}_{BBR_k} \mathbf{W}_{RFR_k} \mathbf{y}_{1,i}(n). \tag{8}$$

On reception of the respective signals, each RRH communicates the same to the BBU pool via wireless fronthaul link.

It is assumed that each RRH and BBU pool follows an analog beamforming structure. Hence, the i-th RRH applies precoder i.e., $\mathbf{V}_i \in \mathbb{C}^{N_T \times N_S}$ to the received signal $\breve{\mathbf{y}}_{1,i}(n)$. Therefore, the transmitted signal from i-th RRH is given as,

$$\mathbf{x}_i(n) = \mathbf{V}_i \breve{\mathbf{y}}_{1,i}(n). \tag{9}$$

The signal vector, denoted by $\mathbf{y}_{BBU}(n) \in \mathbb{C}^{N_R \times 1}$, received at the BBU after processed by the combiner $\mathbf{U}_i \in \mathbb{C}^{N_S \times N_R}$ is given as,

$$\mathbf{y}_{BBU}(n) = \sum_{i=1}^{I} \mathbf{U}_i \Big(\mathbf{H}_{BBU_i} \mathbf{x}_i(n) + \mathbf{w}_{BBU}(n)\Big), \tag{10}$$

where, $\mathbf{w}_{BBU}(n) \in \mathbb{C}^{N_R \times 1} \sim \mathcal{CN}\left(0, \sigma_{w_i}^2\right)$ is the complex additive white Gaussian noise (AWGN) vector at the BBU. $\mathbf{H}_{BBU_i} \in \mathbb{C}^{N_R \times N_T}$ is the mmWave channel matrix between the BBU and i-th RRH. The CSI between each RRH and BBU pool is assumed to be perfectly known. Therefore, the signal received at the BBU pool after perfect channel equalization is given as

$$\breve{\mathbf{y}}_{BBU}(n) = \sum_{i=1}^{I} \breve{\mathbf{y}}_{1,i}(n). \tag{11}$$

In the following section III, we propose a CE scheme, namely L-IVBI, to estimate the desired channel for the pilot contaminated UC-RAN system discussed in the algorithm 1.

On completion of CE at each RRH, the corresponding precoder and combiner of the estimated channel following

algorithms 2 and 3 of section IV are generated, and the same are communicated to UE via the control channel to initiate the data transmission phase.

III. L-IVBI BASED CHANNEL ESTIMATION

This section presents an L-IVBI method for estimating the desired and the sum of the interfering clusters' channel coefficients for the UC-RAN system. The channel gains estimation is performed in the time domain. The proposed method employs an alternative minimization technique to estimate the channel coefficients iteratively. The number of iterations is maintained at a constant value, specifically the minimum number necessary for convergence. Our proposed estimation method comprises two stages: a) Stage-I (Initialization stage)- In this stage, we obtain the coarse estimate of the desired channel employing the least square estimation (LSE) scheme; b) Stage-II (Iteration stage)- Here, the initial CSI estimate of stage-I is iteratively updated using the IVBI technique.

We assume that each UE transmits a N_p length training frame. Let $\mathbf{x}_k^p$ represent the $1 \times N_p$ transmit pilot vector from k-th UE. The unity pilot reuse factor gives rise to pilot contamination i.e., $\mathbf{x}_k^p = \mathbf{x}^p$. Therefore, the received pilot at the i-th RRH of cluster-1 after stacking N_p measurements is given as,

$$\begin{aligned}\mathbf{Y}_{1,i}^p &= \sum_{k=1}^{K} \mathbf{H}_{k,i}\mathbf{X}^p + \mathbf{W}_{1,i} \\ &= \mathbf{H}_{1,i}\mathbf{X}^p + \sum_{k=2}^{K} \mathbf{H}_{k,i}\mathbf{X}^p + \mathbf{W}_{1,i}. \end{aligned} \tag{12}$$

After vectorization of (12), the received pilot is represented as,

$$\begin{aligned}\mathbf{y}_{1,i}^p &= \sum_{k=1}^{K} \Phi\mathbf{g}_{k,i} + \mathbf{w}_{k,i} \\ &= \underbrace{\Phi\mathbf{g}_{1,i}}_{\text{target cluster}} + \underbrace{\Phi\mathbf{g}_{int}}_{\text{interfering clusters}} + \mathbf{w}_{k,i}. \end{aligned} \tag{13}$$

In (13), $\Phi = ((\mathbf{X}^p)^T \otimes \mathbf{I}_{N_R}) \times (\text{conj}(\mathbf{A}_T) \otimes \mathbf{A}_R)$, $\mathbf{g}_{int} = \sum_{k=2}^{K} \mathbf{g}_{k,i}$ and $\mathbf{g}_{k,i} = \text{vec}\,(\beta_{k,i}^{1/2}\mathbf{G}_{k,i})$.

We propose an L-IVBI-based method for estimating the desired and interfering channels. Hence, RRH employs the estimation of the channels $\mathbf{g}_{1,i}$ and $\mathbf{g}_{int}$ from the received pilot signal using the IVBI method mentioned in Algorithm 1.

A. INITIALIZATION STAGE

We employ LSE based estimation scheme to obtain the initial estimate (i.e. $m = 0$) of channel $\mathbf{g}_{1,i}$ (i.e., $\hat{\mathbf{g}}_{1,i}^{[0]}$) from the received pilot $\mathbf{y}_{1,i}^p$ given in (13). Therefore the initial estimate $\hat{\mathbf{g}}_{1,i}^{[0]}$ is as follows

$$\hat{\mathbf{g}}_{1,i}^{[0]} = (\Phi^H\Phi)^{-1}\Phi^H\mathbf{y}_{1,i}^p. \tag{14}$$

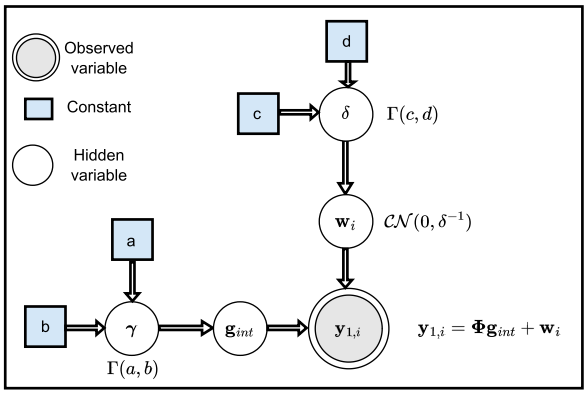

FIGURE 4. Graphical model for VBI approach.

B. ITERATION STAGE

On completion of the coarse estimation $\hat{\mathbf{g}}_{1,i}^{[0]}$, an iterative algorithm is proposed to fine-tune the estimate of $\mathbf{g}_{1,i}$ employing IVBI method. Eliminating the estimated $\hat{\mathbf{g}}_{1,i}^{[0]}$ from the received signal (13), the resultant signal, $\check{\mathbf{y}}_{1,i}^{[m]}$, is expressed as,

$$\check{\mathbf{y}}_{1,i}^{[m]} = \Phi\mathbf{g}_{int}^{[m]} + \mathbf{w}_{k,i}, \tag{15}$$

where m is the m-th iteration stage. Now, with the knowledge of $\check{\mathbf{y}}_{1,i}^{[m]}$ and Φ, estimation of $\mathbf{g}_{int}^{[m]}$ (i.e. $\hat{\mathbf{g}}_{int}^{[m]}$) is carried out following the steps 4 to 15 of Algorithm 1. To promote sparsity, we utilize a two-layer hierarchical Gaussian-inverse Gamma prior model to estimate the value of $\mathbf{g}_{int}$. The VBI graphical model is presented in Fig. 4 for the given signal model in (15). We assume that in the first layer, the non-zero values of channel vector $\mathbf{g}_{int}$, i.e. $(g_{int_n} \mid \gamma_n) \in n = 1, .., N_B$, are independent and identically distributed (i.i.d) and follow complex Gaussian distribution with zero mean in the first layer simplifies calculations and offers flexibility. Hence,

$$\begin{aligned} p(\mathbf{g}_{int} \mid \boldsymbol{\gamma}) &= \prod_{n=1}^{N_B} \mathcal{N}(g_{int_n} \mid 0, \gamma_n^{-1}) \\ &= \frac{1}{(2\pi)^{N_B/2}\left|\tilde{\mathbf{A}}\right|^{-1/2}} \exp\left(-\frac{1}{2}\mathbf{g}_{int}^H\tilde{\mathbf{A}}\mathbf{g}_{int}\right), \end{aligned} \tag{16}$$

where, the channel sparsity is denoted by $\tilde{\mathbf{A}} = \text{diag}(\boldsymbol{\gamma})$. The set of non-negative hyperparameters that regulates the sparsity of $\mathbf{g}_{int}$ is represented as $\boldsymbol{\gamma} = [\gamma_1, \gamma_2, \ldots, \gamma_{N_B}]^T$, where $N_B = G_R \times G_T$. In the second layer, the Gamma distribution is chosen to serve as the hyperprior for the hyperparameter γ, i.e., $p(\gamma_n) = \Gamma(\gamma_n \mid a, b)$, with a and b being small constant values employed to ensure that these priors remain non-informative with respect to $\boldsymbol{\gamma}$. It is assumed that in (13), $\mathbf{w}_{k,i} \in \mathcal{N}(0, \delta^{-1})$. Therefore, the hyper-prior for the hyper-parameter δ is given by $p(\delta) = \Gamma(\delta \mid c, d)$. The parameters c, d are small constant values to make the prior non-informative. The set of the unobserved variables $\{\mathbf{g}_{int}, \boldsymbol{\gamma}, \delta\}$ is represented by $\{\mathbf{z}\}$. The log-marginal

probability of $\mathbf{y_{1,i}}$, i.e. $\ln p(\mathbf{y_{1,i}})$ is decomposed into two terms since the direct computation of $p(\mathbf{z}|\mathbf{y_{1,i}})$ is difficult given as,

$$\ln p(\mathbf{y_{1,i}}) = L(q) + KL(q||p). \tag{17}$$

In (17),

$$L(q) = L(q_n q_{\bar{n}}) = \int q(\mathbf{z}) \ln(\frac{p(\mathbf{y_{1,i}}, \mathbf{z})}{q(\mathbf{z})}) d\mathbf{z},$$
$$KL(q||p) = -\int q(\mathbf{z}) \ln(\frac{p(\mathbf{z}|\mathbf{y_{1,i}})}{q(\mathbf{z})}) d\mathbf{z}, \tag{18}$$

where $q_{\bar{n}} = \prod_{j \neq n} q_j$ and $q(\mathbf{z})$ is any probability density function (pdf) close to $p(\mathbf{z}|\mathbf{y_{1,i}})$. Since $\mathrm{KL}(q||p) \geq 0$, we find the closest analytical representation of the posterior distribution $p(\mathbf{z}|\mathbf{y_{1,i}})$ by minimizing the KL divergence. The process of minimization of the KL divergence is essentially equivalent to maximizing $L(q)$, as the natural logarithm of $p(\mathbf{y}_{1,i})$ depends solely on $\mathbf{y}_{1,i}$. Therefore, we approximate $p(\mathbf{z}|\mathbf{y}_{1,i})$ by maximizing $L(q)$ while considering the distribution $q(\mathbf{z})$, i.e., $q(\mathbf{g}_{int})$, $q(\boldsymbol{\gamma})$ and $q(\delta)$. Therefore, the Bayesian inference is presented as follows.

1) $q(\mathbf{g}_{int})$**:**

$$q(\mathbf{g}_{int}) = \mathcal{N}(\mathbf{g}_{int} \mid \mu, \Sigma), \tag{19}$$

where, $\Sigma = \left(\langle \delta \rangle \Phi^H \Phi + \left\langle \tilde{\mathbf{A}} \right\rangle \right)^{-1}$ and $\boldsymbol{\mu} = \langle \delta \rangle \Sigma \Phi^H \mathbf{y_{1,i}}$.

2) $q(\boldsymbol{\gamma})$**:** The posterior distribution of $q(\boldsymbol{\gamma})$ is given as,

$$q(\boldsymbol{\gamma}) = \prod_{n=1}^{N_B} \Gamma(\gamma_n \mid \tilde{a}, \tilde{b}_n), \tag{20}$$

where, $\tilde{b}_n = b + \frac{1}{2} \langle g_{1_n} \rangle^2$ and $\tilde{a} = a + \frac{1}{2}$.

3) $q(\delta)$**:** The posterior distribution of $q(\delta)$ is given as,

$$q(\delta) = \Gamma(\delta \mid \tilde{c}, \tilde{d}), \tag{21}$$

where, $\tilde{d} = d + \frac{1}{2} \left\langle \left\| \mathbf{y_{1,i}} - \Phi \mathbf{g}_{int} \right\|^2 \right\rangle^2$ and $\tilde{c} = c + \frac{N_p}{2}$.

The approximate posterior distributions in (19), (20) and (21) are updated iteratively until convergence. Once convergence is achieved, similar steps are followed to evaluate the desired $\hat{\mathbf{g}}_{1,i}^{[m]}$ using the known $\hat{\mathbf{g}}_{int}^{[m]}$.

On completion of the iteration stage, the estimated channel vector $\hat{\mathbf{g}}_{1,i}^{[m+1]}$ is given as,

$$\hat{\mathbf{g}_{1,i}}^{[m+1]} = \boldsymbol{\mu} = \langle \delta \rangle \Sigma \Phi^H \mathbf{y_{1,i}}. \tag{22}$$

Then, the estimated channel $\hat{\mathbf{H}}_{1,i}$ is given as,

$$\hat{\mathbf{H}}_{1,i} = \mathbf{A}_R \mathrm{vec}^{-1}(\hat{\mathbf{g}}_{1,i}^{[m+1]}) \mathbf{A}_T^H. \tag{23}$$

The proposed L-IVBI method is discussed in Algorithm 1. To obtain the estimate of channel, $\hat{\mathbf{g}}_{1,i}^{[0]}$ is initialized following steps 1 to 3. Then steps 5 and 15 are followed for estimating channel $\hat{\mathbf{g}}_{int}^{[m]}$. Steps 16 and 18 are followed to estimate the channel, $\hat{\mathbf{g}}_{1,i}^{[m]}$ utilizing the estimate $\hat{\mathbf{g}}_{int}^{[m]}$. The estimate of the desired channel is updated in step 20.

Algorithm 1 Proposed L-IVBI Algorithm for Pilot Contaminated UC-RAN Systems

Input: Observation $\mathbf{y}_{1,i}$, Φ, $\mathbf{A}_R$, $\mathbf{A}_T$ and tolerance, τ
Output: Estimated channels, $\hat{\mathbf{g}}_{1,i}$ and $\hat{\mathbf{g}}_{int}$

1 **Initialization Stage:**
2 $\mathbf{y}_{1,i} = \Phi \mathbf{g}_{1,i} + \Phi \mathbf{g}_{int} + \mathbf{w}_{1,i}$ from (13)
3 Obtain the coarse estimate of $\hat{\mathbf{g}}_{1,i}^{[0]}$ using $\mathbf{y}_{1,i}$ and Φ as, $\hat{\mathbf{g}}_{1,i}^{[0]} = (\Phi^H \Phi)^{-1} \Phi^H \mathbf{y}_{1,i}$
4 **Iteration Stage:**
5 **for** *iteration* $m = 1, 2, ..$ **do**
6 Calculate $\check{\mathbf{y}}_{1,i} = \mathbf{y}_{1,i} - \Phi \hat{\mathbf{g}}_{1,i}^{[m]}$
7 Initialize: $j = 0$ and a = b = c = d = 10^{-6}
8 Compute the matrix $\Phi = ((\mathbf{X}^p)^T \otimes \mathbf{I}_{N_R})(\mathbf{A}_T^* \otimes \mathbf{A}_R)$
9 **while** $\frac{\left\| \hat{\mathbf{g}}_{int}^{[j]} - \hat{\mathbf{g}}_{int}^{[j-1]} \right\|_2}{\left\| \hat{\mathbf{g}}_{int}^{[j-1]} \right\|_2} < \tau$ *or* $j \leq j_{max}$ **do**
10 $j = j + 1$
11 Update the hyper-parameter δ following (21)
12 Update the hyper-parameter γ following (20)
13 Compute $\hat{\mathbf{g}}_{int}^{[j]}$ using (22)
14 **end**
15 $\hat{\mathbf{g}}_{int}^{[m]} = \hat{\mathbf{g}}_{int}^{[j]}$
16 Calculate updated received pilot, $\check{\mathbf{y}}_{1,i} = \mathbf{y}_{1,i} - \Phi \hat{\mathbf{g}}_{int}^{[m]}$
17 Estimate $\hat{\mathbf{g}}_{1,i}^{[m]}$ using $\check{\mathbf{y}}_{1,i}$ and Φ following similar steps 5 to 14 of the algorithm
18 Update $\hat{\mathbf{g}}_{1,i}^{[m+1]} = \hat{\mathbf{g}}_{1,i}^{[m]}$ and $\hat{\mathbf{g}}_{int}^{[m+1]} = \hat{\mathbf{g}}_{int}^{[m]}$
19 **end**
20 $\hat{\mathbf{H}}_{1,i} = \mathbf{A}_R \mathrm{vec}^{-1}(\hat{\mathbf{g}}_{1,i}^{[m+1]}) \mathbf{A}_T^H$

IV. HYBRID BEAMFORMING-BASED DATA TRANSMISSION

In Section III, we introduce a channel estimation algorithm that leverages the sparse characteristics of the channel. Within this section, we delve into the development of a hybrid beamforming technique essential for the data transmission process, making use of the previously discussed channel estimate $\hat{\mathbf{H}}_{1,i}$ in Section III.

For designing hybrid precoders and combiners in the UC-RAN system, we adopt the OMP-based algorithm [39], which is detailed in Algorithms 2 and 3. These algorithms help us derive both the digital (BB) and analog (RF) precoders by maximizing mutual information, employing the optimal unconstrained precoder $\mathbf{W}_{opt}$ as described in Algorithm 2.

To initiate this process, we begin by performing singular value decomposition (SVD) on the estimated channel matrix, represented as $\hat{\mathbf{H}}_{1,i} = \mathbf{USV}^*$. Here, $\mathbf{U}$ is an $N_R \times$ rank$(\hat{\mathbf{H}}_{1,i})$ unitary matrix, $\mathbf{S}$ is a rank$(\hat{\mathbf{H}}_{1,i}) \times$ rank$(\hat{\mathbf{H}}_{1,i})$ diagonal matrix, containing singular values arranged in decreasing order, and $\mathbf{V}$ is a $N_T \times$ rank$(\hat{\mathbf{H}}_{1,i})$ unitary matrix. We then obtain $\mathbf{W}_{opt}$ as $\mathbf{V}_{:;1:N_S}$. In steps 4-6, we select columns from the RF precoder by considering the transmit array response

Algorithm 2 OMP-Based Hybrid Precoder Generation

Input: W_{opt}, A_T, M_T
Output: W_{BBT}, W_{RFT}
1 $W_{RFT} =$ Empty matrix
2 $W_{resT} = W_{opt}$
3 **for** $n \leq M_T$ **do**
4 $\quad \Psi = A_T^H W_{resT}$
5 $\quad l = \arg\max_{l=1,\ldots,N_{cl}} (\Psi\Psi^H)_{l,l}$
6 $\quad W_{RFT} = [W_{RFT} \mid A_{T(:,l)}]$
7 $\quad W_{BBT} = (W_{RFT}^H W_{RFT})^{-1} W_{RFT}^H W_{opt}$
8 $\quad W_{resT} = \frac{W_{opt} - W_{RFT} W_{BBT}}{\|W_{opt} - W_{RFT} W_{BBT}\|_F}$
9 **end**
10 $W_{BBT} = \sqrt{N_S} \frac{W_{BBT}}{\|W_{RFT} W_{BBT}\|_F}$

Algorithm 3 OMP-Based Hybrid Combiner Generation

Input: $W_{MMSE}, A_R, \mathbf{y}_{1,i}, M_R$
Output: W_{RFR},W_{BBR}
1 $W_{RFR} =$ *Empty matrix*
2 $W_{resR} = W_{MMSE}$
3 **for** $n \leq M_R$ **do**
4 $\quad \Psi = A_R^H \mathbb{E}(\mathbf{y}_{1,i}\mathbf{y}_{1,i}^H) W_{resR}$
5 $\quad l = \arg\max_{l=1,\ldots,N_{cl}} (\Psi\Psi^H)_{l,l}$
6 $\quad W_{RFR} = [W_{RFR} \mid A_{R(:,l)}]$
7 $\quad W_{BBR} =$
$\quad (W_{RFR}^H \mathbb{E}(\mathbf{y}_{1,i}\mathbf{y}_{1,i}^H) W_{RFR})^{-1} W_{RFR}^H \mathbb{E}(\mathbf{y}_{1,i}\mathbf{y}_{1,i}^H) W_{MMSE}$
8 $\quad W_{resR} = \frac{W_{MMSE} - W_{RFR} W_{BBR}}{\|W_{MMSE} - W_{RFR} W_{BBR}\|_F}$
9 **end**

matrix $\mathbf{A}_T$ from Algorithm 2. Finally, in step 7, we compute the unnormalized transmit baseband (BB) precoder as $W_{BBT} = (W_{RFT}^H W_{RFT})^{-1} W_{RFT}^H W_{opt}$. The residue, $\mathbf{W}_{\text{resT}} = \frac{W_{opt} - W_{RFT} W_{BBT}}{\|W_{opt} - W_{RFT} W_{BBT}\|_F}$ is calculated following steps 8. The BB precoder is normalized in step 10.

Subsequently, we proceed with the design of hybrid combiners as outlined in Algorithm 3. These hybrid combiners are formulated by minimization of the mean square error (MSE) between the processed received and transmitted symbols. Initially, we obtain the optimal unconstrained matrix $\mathbf{W}_{\text{MMSE}}$ that minimizes the MSE between the processed received and transmitted symbols. Similar to the precoder design, we select columns from the RF combiner by considering the columns of $\mathbf{A}_R$, following steps 4-6 of Algorithm 3. The BB combiner, denoted as W_{BBR}, is computed in step 7 as follows: $W_{BBR} = (W_{RFR}^H \mathbb{E}(\mathbf{y}_{1,i}\mathbf{y}_{1,i}^H) W_{RFR})^{-1} W_{RFR}^H \mathbb{E}(\mathbf{y}_{1,i}\mathbf{y}_{1,i}^H) W_{MMSE}$. Finally, in step 8 of the algorithm, we determine the residue $\mathbf{W}_{resR}$ using the expression: $\frac{W_{MMSE} - W_{RFR} W_{BBR}}{|W_{MMSE} - W_{RFR} W_{BBR}|_F}$.

Upon calculating the precoders and combiners, the data transmission process is initiated following the hybrid beamforming architecture.

The signal-to-interference-and-noise ratio (SINR) of the signal received at the BBU is calculated from (10) as follows,

$$\boldsymbol{\gamma}_{BBU} = \frac{\sum_{i=1}^{I} \Omega_{i,k} \Omega_{i,k}^H}{\sum_{i=1}^{I} (\sum_{j=1, j\neq k}^{K} \Omega_{i,j} \Omega_{i,j}^H + \sigma_{w_i}^2 \mathbf{W}_R^H \mathbf{W}_R)}, \tag{24}$$

where, $\Omega_{i,k} = \mathbf{W}_{BBR_k}^H \mathbf{W}_{RFR_k}^H \hat{\mathbf{H}}_{i,k} \mathbf{W}_{RFT_k} \mathbf{W}_{BBT_k}$ and $\mathbf{W}_R = \mathbf{W}_{RFR_k} \mathbf{W}_{BBR_k}$.

Thus, the spectral efficiency (SE) for the proposed system at the BBU pool discussed in V-B is given by,

$$R = \log_2 \left| \mathbf{I} + \boldsymbol{\gamma}_{BBU} \right|. \tag{25}$$

A. BAYESIAN CRAMÉR RAO BOUND

In this section, we determine the BCRB for the UC-RAN system. For the for the channel matrix, $\mathbf{g}$, the Bayesian Fisher Information Matrix (FIM), $\mathbf{J}$, is expressed as,

$$\mathbf{J} = \mathbf{J}_{\tilde{\mathbf{y}_{k,i}} | g_{k,i}} + \mathbf{J}_{\mathbf{g}_{k,i}}, \tag{26}$$

where,

$$\mathbf{J}_{\tilde{\mathbf{y}_{k,i}} | g_{k,i}} = -\mathbb{E}\left[\frac{\partial^2 \ln p(\tilde{\mathbf{y}_{k,i}} \mid \mathbf{g}_{k,i})}{\partial \mathbf{g}_{k,i}^2} \right], \tag{27}$$

and

$$\mathbf{J}_{\mathbf{g}_{k,i}} = \left(\frac{\partial \ln p(\mathbf{g}_{k,i})}{\partial \mathbf{g}_{k,i}} \right)^H \left(\frac{\partial \ln p(\mathbf{g}_{k,i})}{\partial \mathbf{g}_{k,i}} \right). \tag{28}$$

In (27), $\ln p(\tilde{\mathbf{y}_{k,i}} \mid \mathbf{g})$ denotes the log-likelihood of the measurement vector expressed as,

$$\begin{aligned} &\ln p(\tilde{\mathbf{y}_{k,i}} \mid \mathbf{g}_{k,i}) \\ &= \text{constant} - (\tilde{\mathbf{y}_{k,i}} - \Phi \mathbf{g}_{k,i})^H \mathbf{C}^{-1} (\tilde{\mathbf{y}_{k,i}} - \Phi \mathbf{g}_{k,i}), \end{aligned} \tag{29}$$

with $\mathbf{C} = \sigma_{w_{k,i}}^2 \mathbf{I}_{N_R}$. Hence, we can obtain $\mathbf{J}_{\tilde{\mathbf{y}_{k,i}} | g_{k,i}} = \Phi^H \mathbf{C}^{-1} \Phi$. The actual prior distribution $p(\mathbf{g}_{k,i}; a, b)$ for the sparse channel matrix $\mathbf{g}_{k,i}$ simplifies to the following:

$$\begin{aligned} p(\mathbf{g}_{k,i}; a, b) &= \int p(\mathbf{g}_{k,i} \mid \boldsymbol{\gamma}) p(\boldsymbol{\gamma}; a, b) d\boldsymbol{\gamma} \\ &= \int \prod_{n=1}^{N_B} \mathcal{N}(g_{k,i_n} \mid 0, \boldsymbol{\gamma}_n^{-1}) \Gamma(\boldsymbol{\gamma}_n \mid a, b) d\boldsymbol{\gamma}_n \\ &= \prod_{n=1}^{N_B} St(g_{k,i_n} \mid \xi, \lambda, \varsigma), \end{aligned} \tag{30}$$

where, $St(g_{k,i_n} \mid \xi, \lambda, \varsigma)$ is a Student-t distribution with $\lambda = \frac{a}{b}$, $\xi = 0$, $\varsigma = 2a$ and is expressed as,

$$St(g_{k,i_n} \mid \xi, \lambda, \varsigma) = \frac{\Gamma((\varsigma+1)/2)}{\Gamma(\varsigma/2)} \left(\frac{\lambda}{\pi\varsigma}\right)^{1/2} \left(\frac{\Xi}{\varsigma}\right)^{-\frac{\varsigma+1}{2}}, \tag{31}$$

where, $\Xi = \varsigma + \lambda(g_{k,i_n} - \xi)^2$. The prior distribution of g_{k,i_n} is obtained as,

$$p(g_{k,i_n}) = St(g_{k,i_n} \mid \xi, \lambda, \varsigma). \tag{32}$$

The log-likelihood function of $p(g_{k,i_n})$ is given as,

$$L(g_{k,i_n}) = \ln\frac{\varsigma-1}{\varsigma-2} - \frac{1}{2}\ln\pi\varsigma + \frac{\varsigma+1}{2}\ln\varsigma + \frac{1}{2}\ln\lambda - \frac{\varsigma+1}{2}\ln\Xi. \tag{33}$$

The first-order derivative of $L(g_{k,i_n})$ is expressed as,

$$U(g_{k,i_n}) = \Big[-\frac{(\varsigma+1)g_{k,i_n}\lambda}{\Xi}, \frac{1}{2\lambda} - \frac{(\varsigma+1)g_{k,i_n}^2}{2\Xi}, \frac{1}{2}\ln(\frac{\varsigma}{\Xi}) + \frac{\lambda g_{k,i_n}^2 - 1}{2\Xi} - \frac{1}{(\varsigma-1)(\varsigma-2)}\Big]^H. \tag{34}$$

$\mathbf{J}_{\mathbf{g}_{k,i}}$ is given as,

$$\mathbf{J}_{\mathbf{g}_{k,i}} = U(\mathbf{g}_{k,i})^H U(\mathbf{g}_{k,i}), \tag{35}$$

with $U(\mathbf{g}_{k,i}) = \sum_{n=1}^{N} U(g_{k,i_n})$. Therefore, the BCRB for channel $\mathbf{g}_{k,i}$ is hence given as,

$$\text{BCRB}(\mathbf{g}_{k,i}) = \text{Tr}(\mathbf{J}^{-1}). \tag{36}$$

B. COMPLEXITY ANALYSIS

The computational complexity of an algorithm is determined by counting the total number of complex additions and multiplications involved. The generalized complexity of the proposed estimator is given as,

$$\mathcal{C} = \mathcal{O}(\mathcal{C}_{ini} + \mathcal{C}_{iter}), \tag{37}$$

where $\mathcal{O}(\mathcal{C}_{ini})$ is the complexity of the initialization stage. For L-IVBI, the $\mathcal{O}(\mathcal{C}_{ini}) = \mathcal{O}(\mathcal{C}_{ini_{L-IVBI}})$ is given by $2N_pG_RG_T^2$. The second term $\mathcal{O}(\mathcal{C}_{iter})$ corresponds to the complexity of the iteration stage. Therefore, $\mathcal{O}(\mathcal{C}_{iter})$ for m-th iteration for the method involve calculation of the covariance matrix $\Sigma \in \mathbb{C}^{G_RG_T \times G_RG_T}$ in (19). Therefore, $\mathcal{O}(\mathcal{C}_{iter}) = G_R^3G_T^3$ denotes the computational complexity associated with the iteration stage. The computational complexity associated with estimating channel gains using CoSaMP is expressed as $\mathcal{O}(G_TG_RN_RN_p)$. Considering $G_R = G_T = 16$, $N_p = 100$, the $\mathcal{O}(\mathcal{C}_{ini}) = \mathcal{O}(8, 19, 200)$ and $\mathcal{O}(\mathcal{C}_{iter}) = \mathcal{O}(1, 67, 77, 216)$. Therefore, the computational complexity for m-th iteration of L-IVBI is given as $\mathcal{O}(1, 67, 77, 216)$ whereas the complexity of CoSaMP is $\mathcal{O}(G_TG_RN_RN_p) = \mathcal{O}(4, 09, 600)$. Hence, the proposed estimation method has a higher computational complexity but improves performance in NMSE, SE, and BER.

V. RESULTS AND DISCUSSIONS

In this section, we provide simulation results that evaluate the effectiveness of the proposed channel estimator within the context of the UC-RAN system. We assume that each RRH within the UC-RAN system is equipped with a variable number of receiving antennas, denoted as N_R, and taking values within the range (16, 64, 128). Additionally, each UE is considered to have a single transmitting antenna, denoted as $N_T = 1$. Parameters $N_S = 1$, $M_T = 1$, and $M_R = 4$ represent the number of data streams, transmit RF chains, and receive RF chains, respectively.

It's important to mention that we assume a particular antenna array setup in which the separation between neighboring antenna elements is precisely half of the wavelength associated with the operational frequency. The mmWave channel is generated using a model with $N_{cl} = 4$ scatterers, and we assume an ideal mmWave channel with no grid mismatch. For the VBI process, we configure the maximum number of iterations as $j_{max} = 100$ and set the stopping tolerance τ to 10^{-10}.

We distribute equal power across the parallel streams, and the data symbols are modulated using Quadrature Phase Shift Keying (QPSK). The pilot signal employed is the Zadoff-Chu (ZC) sequence. For a comprehensive overview of the simulation parameters, please refer to Table 1.

TABLE 1. Simulation parameters.

Parameter	Value
N_R	$(16, 64, 128)$
N_T	1
G_T	16
G_R	$(16, 32, 64)$
M_T	1
M_R	4
N_S	1
Number of UEs, K	$(2, 4)$
$\beta_{k,i}$	$(1, 0.1)$
N_p	100
N_{cl}	4
tolerance, τ	10^{-10}
α_l, follows	$\mathcal{CN}(0, 1)$
Pilot sequence	Zadoff-Chu (ZC)
maximum iteration for VBI, j_{max}	100
Monte-Carlo iteration	1000
Modulation	QPSK

The simulation outcomes are averaged across 1000 Monte-Carlo iterations to ensure a reliable and statistically robust assessment.

The NMSE is expressed as

$$\text{NMSE} = \mathbb{E}\left[\frac{\left\|\hat{\mathbf{H}}_{k,i} - \mathbf{H}_{k,i}\right\|_F^2}{\left\|\mathbf{H}_{k,i}\right\|_F^2}\right], \tag{38}$$

where, $\mathbf{H}_{k,i}$ and $\hat{\mathbf{H}}_{k,i}$ denote the true and estimated channels respectively. The SNR at the transmitter side is defined as $\frac{p_k}{\sigma_{w_i}^2}$. We employ state-of-the-art estimator compressive sampling matching pursuit (CoSaMP) [40] and minimum mean squared error (MMSE) [41] for comparison, where the results are regenerated as per the system model. Additionally, we demonstrate the SE and BER performance of the UC-RAN system. The algorithm's performance is assessed over various receive antenna size configurations and pilot lengths. We refer the system with $N_R \in (16, 64, 128)$ and $N_T = 1$ as 16×1, 64×1, 128×1 respectively for the simulation.

For comparison, we propose another method called V-IVBI in which the initial estimate of the desired channel $\mathbf{H}_{1,i}$ is obtained by employing the VBI scheme. In this scheme, it is assumed that the first received frame has no/negligible interference from the other clusters, i.e., the i-th RRH receives signal only from the target cluster, i.e., cluster-1. Therefore, the received pilot at the i-th RRH after stacking N_p measurements of the first frame is given as,

$$\mathbf{Y}_{V_{1,i}} = \mathbf{H}_{1,i}\mathbf{X}_1^p + \mathbf{W}_{1,i}, \tag{39}$$

where, $\mathbf{X}_1^p$ represents the $N_T \times N_p$ transmit pilot vector from $\mathbb{UE}_1$. After vectorization of (39), the received pilot is represented as,

$$\mathbf{y}_{V_{1,i}} = \Phi\mathbf{g}_{1,i} + \mathbf{w}_{1,i}. \tag{40}$$

From (40), $\mathbf{g}_{1,i}$ is estimated following the VBI method proposed in section III-B. On obtaining the coarse estimate in the initialization stage, similar iteration stages section III-B are being followed for fine channel estimation.

A. NMSE PERFORMANCE AT RRH

First, we examine the NMSE performance versus the pilot length across different receiver antenna configurations, where N_R takes values from the set 16, 64, 128 at signal-to-noise ratios (SNR) of 20 dB and 0 dB. This analysis is presented in Figure 5. There is a significant improvement in NMSE performance for the proposed L-IVBI method from 10^{-2} to 10^{-4} when N_p increases from 20 to 100. Therefore, a longer pilot length achieves higher accuracy in NMSE. Moreover, for both SNRs, there is a negligible improvement in NMSE after $N_p = 100$. A similar inference can be drawn for the system with a higher N_R. Furthermore, the NMSE variation over N_p for the V-IVBI method is also depicted in Fig. 5 for 20 dB SNR for the three varying numbers of receiver antennas. A similar characteristic is also seen in the L-IVBI method. Moreover, the NMSE performance for varying pilot length in the case of L-IVBI is better than that of the V-IVBI method since L-IVBI can achieve NMSE of 10^{-4} with $N_p = 80$ whereas V-IVBI requires $N_p = 120$ to accomplish the similar NMSE. Therefore, $N_p = 100$ is being considered henceforth as the pilot length unless mentioned otherwise. For the purpose of comparison, NMSE versus N_p for 128 × 1 at SNR of 20 dB is plotted with MMSE and CoSaMP estimator. For CoSaMP, NMSE saturates in the range of 10^{-2} with $N_p \geq 100$. The MMSE estimator performs poorly in estimating the channel gains since it attains NMSE of 0.07 even with the increase in the pilot length. Hence, the proposed L-IVBI scheme outperforms V-IVBI and the state-of-the-art CoSaMP methods.

The iterative phase of Algorithm 1 consists of m iterations. Therefore, it is crucial to assess the convergence of the algorithm that we have proposed. The convergence analysis of 16 × 1 configuration is presented in Fig. 6 for SNR values of 10 and 20 dB. The improvement in NMSE is negligible for $m \geq 3$. Hence, the estimated channel converges

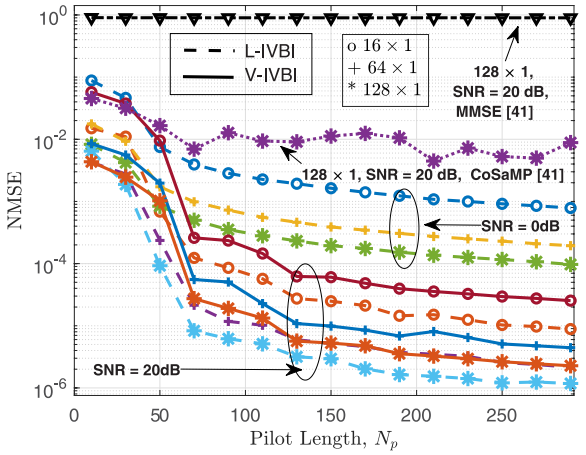

FIGURE 5. NMSE vs. length of pilot performance.

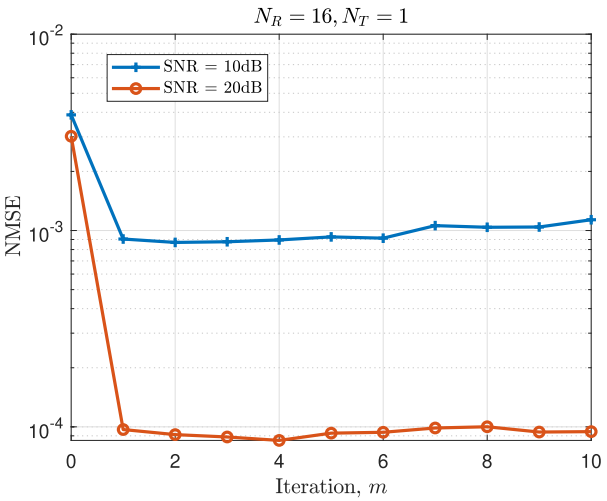

FIGURE 6. Iteration convergence analysis of the proposed algorithm for 16 × 1 configuration.

to its true value within the third iteration, i.e. $m = 3$. This further holds true for all the SNR values. Furthermore, $m = 0$ represents the NMSE performance of the initialization stage. The Initialization stage acquires a coarse channel estimate corresponding to the proposed scheme without the Iterative stage (i.e.,m=0). Comparatively, the Iterative stage notably improves performance by iteratively refining the channel estimate for finer results for both cases. Therefore, $m = 3$ is considered for the rest of the paper.

The next metric of performance analysis is NMSE variation over the number of antennas in RRH, i.e., N_R given in Fig. 7 at 0 dB,10 dB, and 20 dB SNR. As shown in the figure, there is a significant improvement of NMSE when N_R is increased from 8 to 64 for both the proposed method of channel estimation. However, for $N_R \geq 64$, there is a negligible improvement of NMSE over all the SNRs. The proposed L-IVBI estimation scheme can attain higher NMSE over the varying number of RRH antennas than the V-IVBI method. The state-of-the-art MMSE estimator attains NMSE of 0.07 and doesn't improve with the increase in the

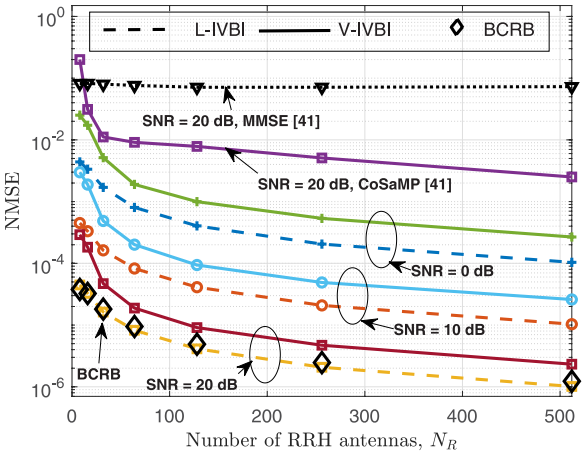

FIGURE 7. NMSE vs N_R performance for various SNR values.

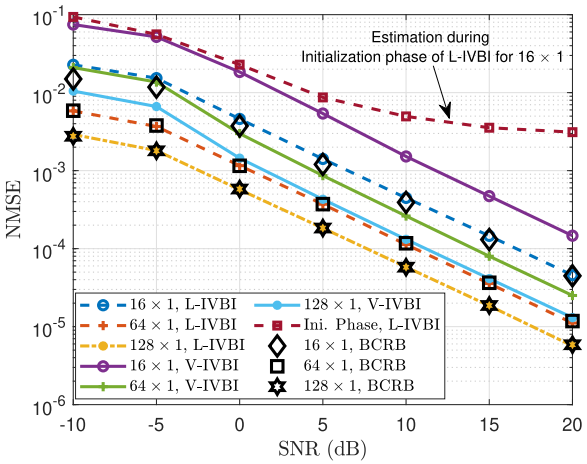

FIGURE 8. NMSE vs. SNR performance.

pilot length. The CoSaMP estimator depicts a similar nature of NMSE performance as that of the proposed estimator for varying antenna sizes. However, it can attain NMSE of 10^{-2} at SNR of 20 dB. Additionally, the BCRB performance for SNR 20 dB is depicted, where it can be observed that the L-IVBI method attains the BCRB.

In Fig. 8, the performance of NMSE versus SNR for different antenna sizes is depicted. The pilot length N_p is set at 100. The L-IVBI method can attain NMSE of 4.6×10^{-5} at 20 dB for 16×1. Further, NMSE performance improves significantly with the increase in the number of transmit and receive antennas from 16×1 to 128×1. Specifically, for the L-IVBI method with 16×1 configuration, NMSE of 10^{-4} is obtained at SNR of 16 dB, whereas similar NMSE is obtained at SNR of 7.5 dB by 128×1. Hence, there is an 8.5 dB SNR improvement with the increase in the number of RRH antennas. Likewise, for the V-IVBI scheme, the improvement in NMSE is seen with the increase in SNR and the increment in the size of RRH antennas. Additionally, L-IVBI, for 128×1, can achieve NMSE 10^{-5} at 17.5 dB, whereas V-IVBI requires about 3.5 dB more SNR to attain similar NMSE. The proposed L-IVBI CE method closely approaches the BCRB performance of all antenna configurations. Furthermore, the NMSE comparison for the Initialization and Iterative stages of the L-IVBI algorithm is shown for 16×1 configuration. At 20 dB, the NMSE achieved by the initialization phase is 0.0031, whereas the iterative phase of L-IVBI improves the NMSE to 4.56×10^{-5}. It is evident that the Iterative stage significantly enhances performance by iteratively refining the channel estimate to provide finer results.

For comparison, we also employ traditional CoSaMP-based algorithms to estimate the channel gains within our simulation setup. We can observe that L-IVBI, for 16×1, attains NMSE of 4.4×10^{-4} at 10 dB whereas, V-IVBI and CoSaMP can achieve NMSE of nearly 1.5×10^{-3} and 1.5×10^{-2}, respectively. However, the MMSE estimator attains NMSE of 0.08 at 20 dB SNR. Thus, the proposed method outperforms the conventional MMSE, CoSaMP, and V-IVBI channel estimators. Additionally, following section IV-A, the performance of the proposed estimation techniques is being evaluated compared to the BCRB. It is seen that the proposed L-IVBI approaches the BCRB more closely at higher SNR.

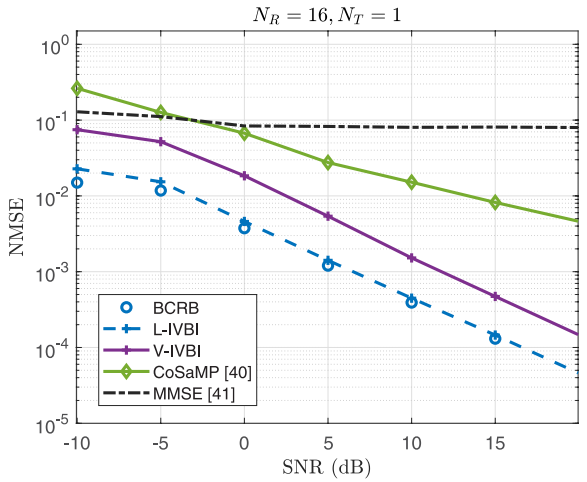

FIGURE 9. NMSE vs. SNR performance.

The relationship between the number of UEs (K) and NMSE for different numbers of receiver antennas (N_R) is shown in Fig. 10. It is observed that with the increase in the number of UEs, the NMSE performance degrades. This is because the interference also increases with the number of UEs. For larger numbers of UEs, the NMSE saturates due to an increase in interference level.

B. SPECTRAL EFFICIENCY PERFORMANCE AT BBU

The next performance measure is the SE attained at the BBU by the pilot-contaminated UC-RAN system, considering the L-IVBI channel estimation approach. The SE vs. SNR for varying N_R configuration is plotted in Fig.11. With the increase in SNR, SE improvement can be observed. A larger

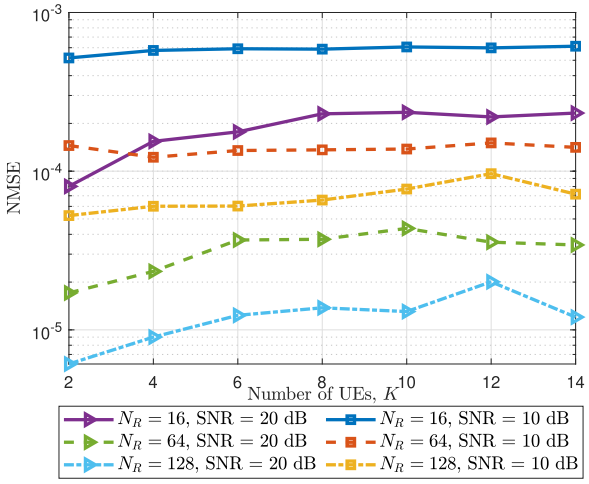

FIGURE 10. NMSE vs. Number of UEs.

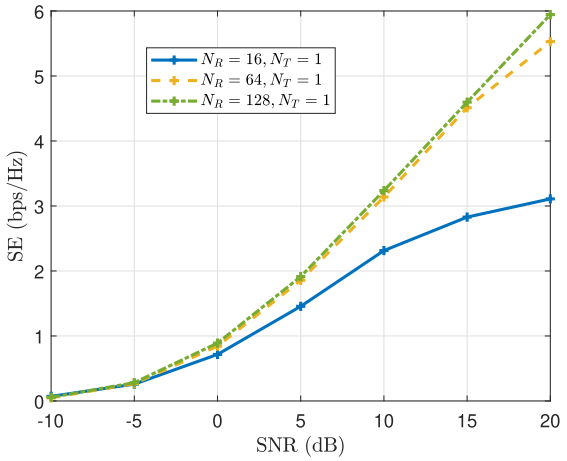

FIGURE 11. SE vs SNR for $K = 2$, $I = 2$.

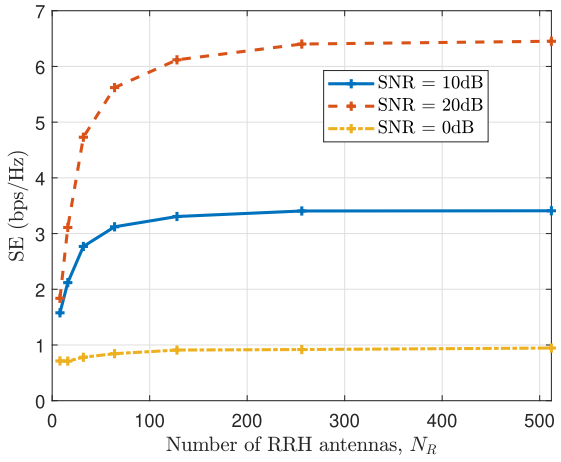

FIGURE 12. SE vs number of RRH antennas N_R at varying SNR.

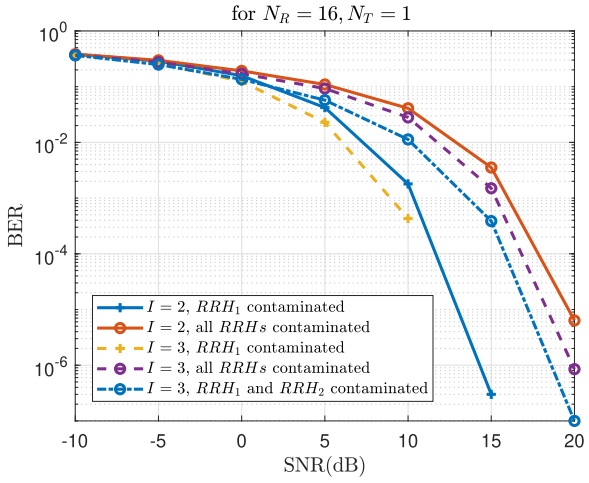

FIGURE 13. BER vs. SNR for varying numbers of contaminated RRHs for 16 × 1 configuration.

antenna size induces more independent paths, thus improving the system's SE. As seen in Fig. 11, the SE of 6 bps/Hz is achieved for 128 × 1 at 20 dB SNR whereas 64 × 1 and 16 × 1 attains SE of 5.52 bps/Hz and 3.1 bps/Hz respectively. However, the increment in SE performance saturates with the increase in the antenna size.

The SE vs. the number of antennas at RRH is plotted in Fig. 12 for varying SNR. It can be observed that there is a significant improvement in the SE from 1.8 bps/Hz to 6 bps/Hz when N_R is increased from 8 to 128 at 20 dB SNR. Even after a further increase in antenna numbers, the SE saturates beyond $N_R = 128$. Similar behavior can be observed over all the SNR conditions.

C. BER PERFORMANCE AT BBU

The BER performance of the system at BBU with L-IVBI estimation is being examined as shown in Fig.13 for 16 × 1 configuration. For this case study, it has been considered that I numbers of RRHs are present in the desired $\mathbb{UE}_k$ cluster, which may or may not be contaminated by neighboring clusters. The BER measurement is performed at BBU, connected to the RRHs via a wireless link. The link between BBU and RRH is assumed to be known. For simplicity, two scenarios are being considered: 1) only one of the RRHs present on the desired cluster is contaminated by the neighboring cluster, and the remaining RRHs are contamination-free, and 2) all the RRHs of the desired cluster are contaminated by the neighboring cluster. It can be observed that there is a significant improvement in BER performance with an increase in the SNR, i.e., BER of 10^{-6} is achieved at 14 dB SNR with $I = 2$ when only one of the RRHs is contaminated. However, the system performance is degraded by 6 dB to achieve BER of 10^{-5} when all the RRHs are contaminated. The system performance can be enhanced by employing more RRHs, as seen for $I = 3$, due to the diversity gain achieved upon employing more RRHs. There is about a 1.5 dB SNR improvement when the number of RRH increases from $I = 2$ to $I = 3$.

VI. CONCLUSION

This paper estimates channel gains for pilot contaminated uplink for the UC-RAN communication system. We have

introduced a channel estimation method based on L-IVBI, which utilizes an alternating minimization approach. The proposed algorithm outperforms the state-of-the-art estimation technique with a reasonable increase in complexity. The numerical results demonstrate the efficacy of the proposed CE method over state-of-the-art channel estimators such as CoSaMP in terms of NMSE. The proposed L-IVBI estimator significantly improves NMSE performance over existing state-of-the-art algorithms. Performance analysis has been demonstrated for different large antenna structures. Furthermore, the SE and BER performance of the UC-RAN system for varying contamination conditions is also addressed. The results demonstrate that, in the presence of pilot contamination, the designed channel estimator significantly improves over the traditional estimator.

REFERENCES

[1] C. Mobile, "C-RAN: The road towards green RAN," China Mobile Res. Inst., White Paper Version 1.0.0, 2011, vol. 2.

[2] M. Peng, C. Wang, J. Li, H. Xiang, and V. Lau, "Recent advances in underlay heterogeneous networks: Interference control, resource allocation, and self-organization," *IEEE Commun. Surveys Tuts.*, vol. 17, no. 2, pp. 700–729, 2nd Quart., 2015.

[3] Y. Shao, Y. Du, Y. Jiang, W. Huang, and K. Sun, "The outage probability analysis of network-centric clustering in C-RAN," in *Proc. IEEE Int. Conf. Artif. Intell. Comput. Appl. (ICAICA)*, Jun. 2021, pp. 224–228.

[4] Ö. T. Demir, E. Björnson, and L. Sanguinetti, "Foundations of user-centric cell-free massive MIMO," 2021, *arXiv:2108.02541*.

[5] A. Checko, H. L. Christiansen, Y. Yan, L. Scolari, G. Kardaras, M. S. Berger, and L. Dittmann, "Cloud RAN for mobile networks—A technology overview," *IEEE Commun. Surveys Tuts.*, vol. 17, no. 1, pp. 405–426, 1st Quart., 2015.

[6] J. Shi, Y. Wang, H. Xu, M. Chen, and B. Champagne, "Performance analysis of user-centric virtual cell dense networks over mmWave channels," in *Proc. IEEE Global Commun. Conf. (GLOBECOM)*, Dec. 2018, pp. 1–7.

[7] J. Shi, C. Pan, W. Zhang, and M. Chen, "Performance analysis for user-centric dense networks with mmWave," *IEEE Access*, vol. 7, pp. 14537–14548, 2019.

[8] B. Zhong, X. Zhu, and E. G. Lim, "Clustering-based pilot assignment for user-centric cell-free mmWave massive MIMO systems," in *Proc. IEEE 96th Veh. Technol. Conf. (VTC-Fall)*, Sep. 2022, pp. 1–5.

[9] S. Buzzi, C. D'Andrea, M. Fresia, and X. Wu, "Multi-UE multi-AP beam alignment in mmWave cell-free massive MIMO exploiting channel sparsity," in *Proc. 25th Int. ITG Workshop Smart Antennas*, Nov. 2021, pp. 1–6.

[10] X. Zhang, J. Wang, and H. V. Poor, "Statistical delay/error-rate bounded QoS provisioning across clustered mmWave-channels over cell-free massive MIMO based 5G mobile wireless networks in the finite blocklength regime," in *Proc. 54th Annu. Conf. Inf. Sci. Syst. (CISS)*, Mar. 2020, pp. 1–6.

[11] G. Wang, Q. Liu, R. He, F. Gao, and C. Tellambura, "Acquisition of channel state information in heterogeneous cloud radio access networks: Challenges and research directions," *IEEE Wireless Commun.*, vol. 22, no. 3, pp. 100–107, Jun. 2015.

[12] M. Peng, Y. Sun, X. Li, Z. Mao, and C. Wang, "Recent advances in cloud radio access networks: System architectures, key techniques, and open issues," *IEEE Commun. Surveys Tuts.*, vol. 18, no. 3, pp. 2282–2308, 3rd Quart., 2016.

[13] M. Attarifar, A. Abbasfar, and A. Lozano, "Random vs structured pilot assignment in cell-free massive MIMO wireless networks," in *Proc. IEEE Int. Conf. Commun. Workshops (ICC Workshops)*, May 2018, pp. 1–6.

[14] H. A. Ammar, R. Adve, S. Shahbazpanahi, G. Boudreau, and K. V. Srinivas, "Downlink resource allocation in multiuser cell-free MIMO networks with user-centric clustering," *IEEE Trans. Wireless Commun.*, vol. 21, no. 3, pp. 1482–1497, Mar. 2022.

[15] H. A. Ammar, R. Adve, S. Shahbazpanahi, G. Boudreau, and K. Srinivas, "Resource allocation and scheduling in non-coherent user-centric cell-free MIMO," in *Proc. IEEE Int. Conf. Commun.*, Jun. 2021, pp. 1–6.

[16] H. Masoumi, M. Javad Emadi, and S. Buzzi, "Cell-free massive MIMO with underlaid D2D communications and low resolution ADCs," 2020, *arXiv:2005.10068*.

[17] H. Q. Ngo, A. Ashikhmin, H. Yang, E. G. Larsson, and T. L. Marzetta, "Cell-free massive MIMO versus small cells," *IEEE Trans. Wireless Commun.*, vol. 16, no. 3, pp. 1834–1850, Mar. 2017.

[18] H. Liu, J. Zhang, S. Jin, and B. Ai, "Graph coloring based pilot assignment for cell-free massive MIMO systems," *IEEE Trans. Veh. Technol.*, vol. 69, no. 8, pp. 9180–9184, Aug. 2020.

[19] X. Zhu, L. Dai, and Z. Wang, "Graph coloring based pilot allocation to mitigate pilot contamination for multi-cell massive MIMO systems," *IEEE Commun. Lett.*, vol. 19, no. 10, pp. 1842–1845, Oct. 2015.

[20] Z. Chen, X. Hou, and C. Yang, "Training resource allocation for user-centric base station cooperation networks," *IEEE Trans. Veh. Technol.*, vol. 65, no. 4, pp. 2729–2735, Apr. 2016.

[21] A. Ashikhmin, H. Q. Ngo, T. L. Marzetta, and H. Yang, "Pilot assignment in cell free massive MIMO wireless systems," U.S. Patent 9 384 615, Apr. 4, 2017.

[22] T. C. Mai, H. Q. Ngo, M. Egan, and T. Q. Duong, "Pilot power control for cell-free massive MIMO," *IEEE Trans. Veh. Technol.*, vol. 67, no. 11, pp. 11264–11268, Nov. 2018.

[23] A. Almamori and S. Mohan, "Estimation of channel state information (CSI) in cell-free massive MIMO based on time of arrival (ToA)," *Wireless Pers. Commun.*, vol. 114, no. 2, pp. 1825–1831, Sep. 2020.

[24] P. Liu, S. Jin, T. Jiang, Q. Zhang, and M. Matthaiou, "Pilot power allocation through user grouping in multi-cell massive MIMO systems," *IEEE Trans. Commun.*, vol. 65, no. 4, pp. 1561–1574, Apr. 2017.

[25] G. Interdonato, H. Q. Ngo, E. G. Larsson, and P. Frenger, "How much do downlink pilots improve cell-free massive MIMO?" in *Proc. IEEE Global Commun. Conf. (GLOBECOM)*, Dec. 2016, pp. 1–7.

[26] Y. Jin, J. Zhang, S. Jin, and B. Ai, "Channel estimation for cell-free mmWave massive MIMO through deep learning," *IEEE Trans. Veh. Technol.*, vol. 68, no. 10, pp. 10325–10329, Oct. 2019.

[27] K. Zhang, W. Zuo, and L. Zhang, "FFDNet: Toward a fast and flexible solution for CNN-based image denoising," *IEEE Trans. Image Process.*, vol. 27, no. 9, pp. 4608–4622, Sep. 2018.

[28] Y. Jin, J. Zhang, B. Ai, and X. Zhang, "Channel estimation for mmWave massive MIMO with convolutional blind denoising network," *IEEE Commun. Lett.*, vol. 24, no. 1, pp. 95–98, Jan. 2020.

[29] G. Interdonato, P. Frenger, and E. G. Larsson, "Utility-based downlink pilot assignment in cell-free massive MIMO," in *Proc. 22nd Int. ITG Workshop Smart Antennas*, Mar. 2018, pp. 1–8.

[30] C. Qing, L. Dong, L. Wang, J. Wang, and C. Huang, "Joint model and data-driven receiver design for data-dependent superimposed training scheme with imperfect hardware," *IEEE Trans. Wireless Commun.*, vol. 21, no. 6, pp. 3779–3791, Jun. 2022.

[31] C. Qing, L. Wang, L. Dong, and J. Wang, "Enhanced ELM based channel estimation for RIS-assisted OFDM systems with insufficient CP and imperfect hardware," *IEEE Commun. Lett.*, vol. 26, no. 1, pp. 153–157, Jan. 2022.

[32] C. Qing, L. Dong, L. Wang, G. Ling, and J. Wang, "Transfer learning-based channel estimation in orthogonal frequency division multiplexing systems using data-nulling superimposed pilots," *PLoS One*, vol. 17, no. 5, May 2022, Art. no. e0268952.

[33] H. Yin, D. Gesbert, M. Filippou, and Y. Liu, "A coordinated approach to channel estimation in large-scale multiple-antenna systems," *IEEE J. Sel. Areas Commun.*, vol. 31, no. 2, pp. 264–273, Feb. 2013.

[34] J. Lee, G.-T. Gil, and Y. H. Lee, "Channel estimation via orthogonal matching pursuit for hybrid MIMO systems in millimeter wave communications," *IEEE Trans. Commun.*, vol. 64, no. 6, pp. 2370–2386, Jun. 2016.

[35] Y. Ding, S.-E. Chiu, and B. D. Rao, "Bayesian channel estimation algorithms for massive MIMO systems with hybrid analog-digital processing and low-resolution ADCs," *IEEE J. Sel. Topics Signal Process.*, vol. 12, no. 3, pp. 499–513, Jun. 2018.

[36] J. Wang, J. Yi, R. Han, L. Bai, and J. Choi, "Variational Bayesian inference for channel estimation and user activity detection in C-RAN," *IEEE Wireless Commun. Lett.*, vol. 9, no. 7, pp. 953–956, Jul. 2020.

[37] K. Liu, X. Li, J. Fang, and H. Li, "Bayesian mmWave channel estimation via exploiting joint sparse and low-rank structures," *IEEE Access*, vol. 7, pp. 48961–48970, 2019.

[38] D. G. Tzikas, A. C. Likas, and N. P. Galatsanos, "The variational approximation for Bayesian inference," *IEEE Signal Process. Mag.*, vol. 25, no. 6, pp. 131–146, Nov. 2008.
[39] O. E. Ayach, S. Rajagopal, S. Abu-Surra, Z. Pi, and R. W. Heath, "Spatially sparse precoding in millimeter wave MIMO systems," *IEEE Trans. Wireless Commun.*, vol. 13, no. 3, pp. 1499–1513, Mar. 2014.
[40] D. Needell and J. A. Tropp, "CoSaMP: Iterative signal recovery from incomplete and inaccurate samples," *Appl. Comput. Harmon. Anal.*, vol. 26, no. 3, pp. 301–321, May 2009.
[41] D. Neumann, T. Wiese, and W. Utschick, "Learning the MMSE channel estimator," *IEEE Trans. Signal Process.*, vol. 66, no. 11, pp. 2905–2917, Jun. 2018.

SOUMYASREE BERA (Graduate Student Member, IEEE) received the B.Tech. and M.Tech. degrees in electronics and communication engineering from Sikkim Manipal Institute of Technology, Sikkim Manipal University, in 2011 and 2015, respectively. She is currently pursuing the Ph.D. degree in telecommunication engineering with Indian Institute of Technology at Kharagpur, Kharagpur, India.

Her research interests include 5G/6G communications, millimeter wave communications, terahertz communications, and integrated sensing and communication.

VENU BALAJI VINNAKOTA received the B.Tech. degree in electronics and communication engineering from Jawaharlal Nehru Technological University, Hyderabad, and the M.Tech. degree in advanced communication systems from NIT Warangal. He is currently pursuing the Ph.D. degree with the G S Sanyal School of Telecommunications, Indian Institute of Technology at Kharagpur, Kharagpur, India. His research interests include applying stochastic geometry analysis to user-centric cloud radio access networks, mmWave channel estimation, and green wireless communications.

DEBARATI SEN (Senior Member, IEEE) received the Ph.D. degree in telecommunication engineering from Indian Institute of Technology at Kharagpur, Kharagpur, India, in 2010.

She was a Postdoctoral Research Fellow with Chalmers University of Technology, Gothenburg, Sweden, and a Senior Chief Engineer with the Samsung Research and Development Institute India, Bengaluru, India. She is currently an Associate Professor with Indian Institute of Technology at Kharagpur. Her research interests include wireless and optical communication systems, mostly on MB-OFDM, synchronization, equalization, UWB, BAN, green communications, 60-GHz communications, and baseband algorithm design for coherent optical communications. She is an editorial board member of two international journals. She was a recipient of the Best Paper Award at Samsung Tech. Conference 2010, the IEI Young Engineers Award 2010, the IETE N. V. G. Memorial Award in 2013, the DAAD-IIT Faculty Exchange Fellowship in 2014, and the Qualcomm Innovation Fellowship in 2017.